http://www.jmaterenvironsci.com /

JMES

Corrosion inhibition of carbon steel in 1M HCl by 1,5-benzodiazepine derivative: Experimental and molecular modeling studies

Y. El Aoufir[1,2*], J. Sebhaoui[3], H. Lgaz[1,4], Y. El Bakri[3], A. Zarrouk[5], F. Bentiss[6], A. Guenbour[2], E.M. Essassi[3], H. Oudda[1]

[1] *Laboratory of Separation Processes, Faculty of Sciences, University Ibn Tofail, Kenitra, Morocco*
[2] *Laboratory of Nanotechnology, Materials & Environment, Faculty of Sciences, Mohammed V University , Rabat, Morocco*
[3] *Laboratoire de chimie organique heterocyclique, URAC 21, Pôle de compétence pharmacochimie, Université Mohammed V, Faculté des sciences, Rabat, Maroc*
[4]*Laboratory of Applied Chemistry & Environment, ENSA, Ibn Zohr University, PO Box 1136, 80000 Agadir, Morocco*
[5] *LC2AME-URAC 18, Faculty of Science, First Mohammed University, PO Box 717, M-60 000 Oujda, Morocco.*
[6] *Laboratoire de Catalyse et de Corrosion des Matériaux (LCCM), Faculté des Sciences, Université Chouaib Doukkali, BP 20, 24000 El Jadida, Morocco*

Abstract

1,5-Benzodiazepine derivative namely, 4Z-(2-Oxopropyl)-1,3-bis(prop-2-yn-1-yl)-2,3,4,5-tetrahydro-1,5-benzodiazepin-2-one (BZD-1) has been evaluated as corrosion inhibitor for carbon steel in 1M HCl acid by electrochemical impedance spectroscopy (EIS) and potentiodynamic curves techniques. The obtained results showed that BZD-1 is an efficient corrosion inhibitor and an inhibition efficiency of 97% was reached with 1×10^{-3} M of BZD-1. The protection efficiency increased with increasing inhibitor concentration, but the temperature has significantly effect on the inhibition efficiency of BZD-1. Tafel polarization studies revealed that BZD-1 is mixed type inhibitor. The adsorption of BZD-1 on the surface of carbon steel obeyed the Langmuir adsorption isotherm. The adsorption behavior of the BZD-1 on Fe (110) surface was investigated by Monte Carlo simulations to verify its corrosion inhibition steel efficacy. The adsorption energy between inhibitor and carbon steel has been calculated by Monte Carlo simulations.

1. Introduction

The inhibition of carbon steel corrosion of iron in acidic media by different organic compounds has been widely studied[1-18]. The existing literature shows that most of the organic inhibitors act by getting adsorbed on the iron surface. This phenomenon is influenced by the nature and surface charge on metal, the type of aggressive electrolyte and the chemical structure of inhibitor [19-22]. The most well-known acid inhibitors are organic compounds containing nitrogen, sulphur, phosphorus and oxygen atoms [23-25]. The adsorption of these compounds depends on the electronic structure of inhibiting molecules, steric factor, aromaticity and electron density at donor site, presence of functional group, molecular area, molecular weight of the molecule, temperature and electrochemical potential at the metal/solution interface [26-31]. 1,5- Benzodiazepines have these requirements to act as corrosion inhibitors with maximum degree of unsaturation by virtue of the seven membered ring. A review of literature reveals that though there are large numbers of reports on the synthesis and pharmacological activities of benzodiazepine derivatives, only very few works have been carried out on their use as corrosion inhibitors [32,33]. Quantum chemical calculations and Monte Carlo simulations are being used to explain the mechanism of corrosion inhibition [34,35].

The aim of the present investigation is to synthesize a benzodiazepine derivative and evaluate their inhibition performance for carbon steel corrosion in 1 M hydrochloric acid. Potentiodynamic polarization, electrochemical impedance spectroscopic techniques were employed. Quantum chemical calculations and Monte Carlo simulations were performed for the benzodiazepine derivative to complement the experimental results.

2. Experimental details

2.1. Synthesis of the benzodiazepine derivative used as corrosion inhibitor

To a solution of (4Z)-2-oxopropylidene-1, 5-benzodiazepin-2one (0.01 mol) in N,N-dimethylformamid (30 ml), was added K_2CO_3 (0.02 mol), tetra n-butylammonium bromide (0.001 mol) and propargyl bromide (0.02 mol). The reaction mixture was stirred at room temperature for 48 h. The solvent was removed under reduced pressure after filtration. The resulting residue was chromatographed on a silica-gel column using hexane and ethyl acetate (80/20) as eluents to obtain the compound as white crystals. The compound was identified by means of X-Ray data [36].
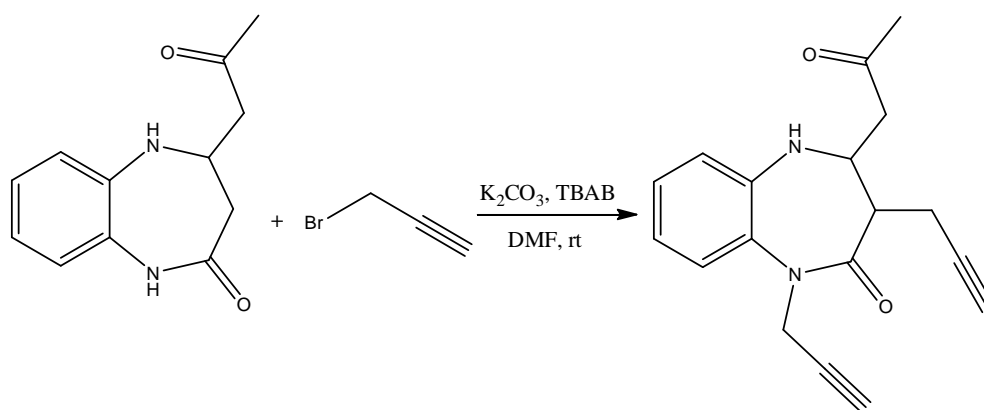
Scheme 1. Synthesis of 4Z-(2-Oxopropyl)-1,3-bis(prop-2-yn-1-yl)-2,3,4,5-tetrahydro-1,5-benzodiazepin-2-one (BZD-1).

2.2. Material

The molecular structure of the BZD-1 is shown in Scheme. 1. The steel used in this study is a carbon steel (Euronorm: C35E carbon steel and US specification: SAE 1035) with a chemical composition (in wt%) of 0.370 % C, 0.230 % Si, 0.680 % Mn, 0.016 % S, 0.077 % Cr, 0.011 % Ti, 0.059 % Ni, 0.009 % Co, 0.160 % Cu and the remainder iron (Fe). the carbon steel sheets were abraded with a series of emery papers SiC (120, 600 and 1200) and then washed with distilled water and acetone.

The aggressive solutions of 1M HCl were prepared by dilution of analytical grade 37% HCl with distilled water. The concentration range of 4Z-(2-Oxopropyl)-1,3-bis(prop-2-yn-1-yl)-2,3,4,5-tetrahydro-1,5-benzodiazepin-2-one (BZD-1) used was 10^{-6} M to 10^{-3} M.

2.3. Electrochemical measurements

The electrochemical measurements were carried out using Volta lab (Tacussel- Radiometer PGZ 100) potentiostate and controlled by Tacussel corrosion analysis software model (Voltamaster 4) at under static condition. The corrosion cell used had three electrodes. The reference electrode was a saturated calomel electrode (SCE). A platinum electrode was used as auxiliary electrode of surface area of 1 cm^2. The working electrode was carbon steel. All potentials given in this study were referred to this reference electrode. The working electrode was immersed in test solution for 30 min to a establish steady state open circuit potential (E_{ocp}). After measuring the E_{ocp}, the electrochemical measurements were performed. All electrochemical tests have been performed in aerated solutions at 303 K. The EIS experiments were conducted in the frequency range with high limit of 100 kHz and different low limit 0.1 Hz at open circuit potential, with 10 points per decade, at the rest potential, after 30 min of acid immersion, by applying 10 mV ac voltage peak-to-peak. Nyquist plots were made from these experiments. The impedance data were analysed and fitted with the simulation ZView 2.80, equivalent circuit software.

After AC impedance tests, the potentiodynamic polarization measurements of carbon steel substrate in inhibited and uninhibited solution were scanned from cathodic to the anodic direction, with a scan rate of 1 mV s^{-1}. The potentiodynamic data were analysed using the polarization VoltaMaster 4 software. The linear Tafel segments of anodic and cathodic curves were extrapolated to corrosion potential to obtain corrosion current densities (I_{corr}). From the polarization curves obtained, the corrosion current (I_{corr}) was calculated by curve fitting using the equation:

$$I = I_{corr}\left[exp\left(\frac{2.3\Delta E}{\beta_a}\right) - exp\left(\frac{2.3\Delta E}{\beta_c}\right)\right] \qquad (1)$$

The inhibition efficiency was evaluated from the measured I_{corr} values using the following relationship:

$$\eta_{Tafel}(\%) = \frac{I_{corr} - I_{corr(i)}}{I_{corr}} \times 100 \qquad (2)$$

where I_{corr} and $I_{corr(i)}$ are the corrosion current densities for steel electrode in the uninhibited and inhibited solutions, respectively.

2.4. Quantum chemical calculations

Complete geometrical optimization of the investigated molecule is performed using reliable $DMol^3$ method implemented in the high-performance software (Materials Studio version 6.0) [37,38]. The GGA is the gradient-corrected functional method was used with a double numeric plus polarization (DNP) basis set and a Becke One Parameter (BOP) functional. The solvation effects (aqueous phase) was included in $DMol^3$ calculations by COSMO[39] controls.

2.5. Monte Carlo simulations

The Monte Carlo (MC) search was adopted to compute the low configuration adsorption energy of the interactions of the BZD-1 on a clean iron surface. The Monte Carlo (MC) simulation was carried out using Materials Studio 6.0 software (Accelrys, Inc.) [38]. The Fe crystal was cleaved along the (110) plane, it is the most stable surface as reported in the literature. Then, the Fe (110) plane was enlarged to (12×12) supercell to provide a large surface for the interaction of the inhibitor. The simulation of the interaction between BZD-1 and the Fe (110) surface was carried out in a simulation box (29.78 × 29.78 × 60.13 Å) with periodic boundary conditions, which modeled a representative part of the interface devoid of any arbitrary boundary effects. After that, a vacuum slab with 30 Å thickness was built above the Fe (110) plane. All simulations were implemented with the COMPASS force field to optimize the structures of all components of the system of interest. More simulation details on the methodology of Monte Carlo simulations can be found in previous publications [40,41].

3. Results and discussion

3.1. Polarization results

The potentiodynamic polarization curves of carbon steel in 1M HCl with and without various concentrations of BZD-1 are shown in Figure 1. Electrochemical parameters extracted from polarization curves including corrosion potential (E_{corr}), cathodic and anodic Tafel slopes (β_c and β_a), corrosion current density (i_{corr}) obtained by extrapolation of the Tafel lines and the calculated η (%) are presented in Table 1.

The presence of increasing amounts of BZD-1 led to a decrease in both the cathodic and anodic current densities. Adsorption is the mechanism that is generally accepted to explain the inhibitory action of organic corrosion inhibitors. The adsorption of inhibitors can affect the corrosion rate in two ways: (i) by decreasing the available reaction area, i.e., the so-called geometric blocking effect, and (ii) by modifying the activation energy of the cathodic and/or anodic reactions occurring in the inhibitor-free metal in the course of the inhibited corrosion process. It is a difficult task to determine which aspects of the inhibiting effect are connected to the geometric blocking action and which are connected to the energy effect. The cathodic Tafel curves in Figure 2 give rise to parallel lines, indicating that the addition of BZD-1 do not modify the hydrogen evolution mechanism and the reduction of hydrogen ions on the carbon steel surface takes place mainly through a charge transfer mechanism [1]. The adsorbed inhibitor molecules only block the active sites of hydrogen evolution on the metal surface. For anodic polarization curves, it is apparent that the benzodiazepine derivative inhibitor performs good inhibition ability between corrosion potential and -300 mV (vs. SCE). However, for potential more positive than -300 mV (vs. SCE), the presence of inhibitor does not alter the current vs. potential characteristics obviously. This potential is usually defined as desorption potential [42]. This phenomenon is generally associated with the significant dissolution of the carbon steel, which leads to desorption of the inhibitor molecules from the electrode surface. In this case, desorption rate of the inhibitor is higher than their adsorption rate[42].
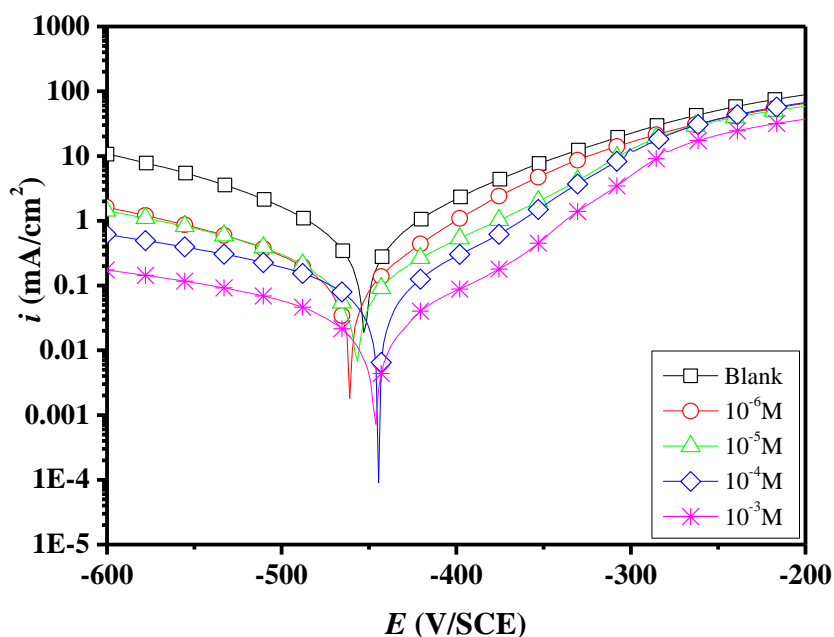
Figure 1: Potentiodynamic polarization curves for carbon steel in 1M HCl solution in the presence and absence of different concentrations of BZD-1 at 303 K.

Table 1: The electrochemical parameters calculated by using the potentiodynamic polarization technique for the corrosion of CS in 1 M HCl in the absence and presence of different concentrations of BZD-1 at 303 K.

Medium	C_{inh} (M)	$-E_{corr}$ (mV/SCE)	I_{corr} ($\mu A\ cm^{-2}$)	β_a (mV dec^{-1})	$-\beta_c$ (mV dec^{-1})	η_{Tafel} (%)
Blank	1	452	507	95.3	113.0	—
BZD-1	10^{-6}	461	124	67.4	107.8	75
	10^{-5}	455	92	76.1	106.5	81
	10^{-4}	444	56	63.9	105.6	88
	10^{-3}	446	19	74.4	117.0	96

As it can be seen from these polarization results, the i_{corr} values decreased considerably in the presence of BZD-1 and decreased with increasing inhibitor concentration. These data show that tested compound is good inhibitor for carbon steel in 1 M HCl solution. We can classify an inhibitor as cathodic or anodic type if the displacement in corrosion potential is more than 85 mV with respect to corrosion potential of the blank[43,44]. In the presence of BZD-1, the corrosion potential of carbon steel shifted to the negative and positive sides less than 85 mV (vs. SCE). This can be interpreted that BZD-1 act as mixed type inhibitor.

### 3.2. Electrochemical impedance spectroscopy (EIS)

Impedance spectra for carbon steel samples in absence and presence of BZD-1 are shown in Figure 2. From Nyquist plots it is evident that the electrochemical response of carbon steel samples appeared in form of depressed capacitive loops, suggesting that a capacitive layer was formed at alloy/acid interface. The diameters of these loops (semicircles) increased with concentration of the benzodiazepine derivative indicating that charge transfer process at the interface retarded in presence of BZD-1.

In the studied frequency range, the system could be described by the corresponding structural model of the interface with BZD-1, as shown in Fig. 3. In this equivalent circuit, R_s is the solution resistance, CPE is the constant phase elements for the double layer and is used instead of a pure capacitor to compensate for non-ideal capacitive response of the interface [45], and R_p is the polarization resistance, where R_p includes charge transfer

resistance (R_{ct}) and the resistance of inhibitor film (R_f) formed on the metal surface in the presence of inhibitor ($R_p = R_{ct} + R_f$) [46]. The impedance (Z) of the CPE is presented by [47]:

$$Z_{CPE} = Q^{-1}(i\omega)^{-n}$$

(3)

where Q is the CPE constant (in Ω^{-1} s^n cm^{-2}), i is the imaginary number, ω is the angular frequency (in rads^{-1}), and n is CPE exponent, which can be used as a gauge heterogeneity or roughness of the surface.
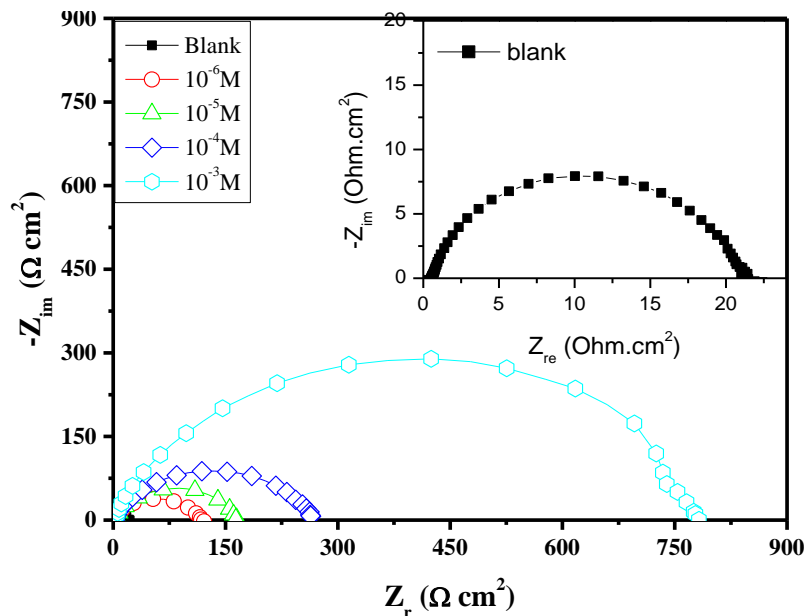
Figure 2: Nyquist plots for carbon steel in 1 M HCl solution containing various concentrations of BZD-1 at 303 K.
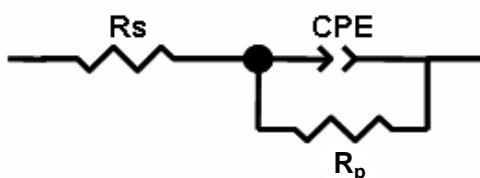
Figure 3: Equivalent electrical circuit corresponding to the corrosion process on the carbon steel in hydrochloric acid.

Table 2 contains all the impedance parameters obtained from the simulation of experimental impedance data, including R_p, Q and n. In the Table 2 are also given the calculated "double layer capacitance" values, C_{dl}, derived from the CPE parameters, using the Hsu and Mansfeld formula [48]:

$$C_{dl} = (Q.R_p^{1-n})^{1/n}$$

(4)

The inhibition efficiency $\eta_Z(\%)$ is calculated by R_p using Eq. 5, R_p and $R_{p(i)}$ were the polarisation resistance of carbon steel electrode in the uninhibited and inhibited solutions, respectively:

$$\eta_Z(\%) = \frac{R_{p(i)} - R_p}{R_{p(i)}} \times 100$$

(5)

The analyse of the results in Table 2 shows that the R_p values increase with increasing concentration of BZD-1 while the C_{dl} values in presence of inhibitor are very lower than that obtained in uninhibited solution, which suggest that the inhibitor adsorb on the steel surface thereby forming a protective layer on the steel surface and reducing the rate of charge transfer process. Also, the values of Q are lower in the presence of BZD-1 compared to that of uninhibited blank system.

Table 2: Impedance parameters recorded for carbon steel electrode in 1M HCl solution in the absence and presence of different concentrations of inhibitor at 303 K.

Medium	$C_{inh.}$ (M)	R_s (Ω cm^2)	R_p (Ω cm^2)	$10^4 Q$ (Ω^{-1}cm^{-2}s^{-n})	n	C_{dl} (μF cm^{-2})	η_Z (%)
Blank	1	0.568	20.24	2.420	0.860	112.04	—
BZD-1	10^{-6}	1.305	113.4	1.620	0.77	49	82
	10^{-5}	1.360	163.6	1.357	0.77	44	87
	10^{-4}	1.495	265.1	0.967	0.76	30	92
	10^{-3}	1.379	775.6	0.483	0.81	22	97

3.3. Adsorption isotherm

The efficiency of the benzodiazepine derivative mainly depends on the adsorption ability on the steel surface. Therefore, it is essential to know the mode of adsorption and the adsorption isotherm which gives information about the interaction between the molecules and metal surface. The degree of surface coverage values (θ) for different concentrations of the benzodiazepine derivative obtained from potentiodynamic polarization measurement were used to fit into different adsorption isotherm models. A plot of C_{inh}/θ vs C_{inh} gives a straight line (Fig. 4) showing that the adsorption of benzodiazepine derivative obeys Langmuir isotherm model which is given by Eq. 6 [49].

$$\frac{C_{inh}}{\theta} = \frac{1}{K_{ads}} + C_{inh} \tag{6}$$

where C_{inh} is the concentration of inhibitor and K_{ads} is the equilibrium constant of the adsorption process.
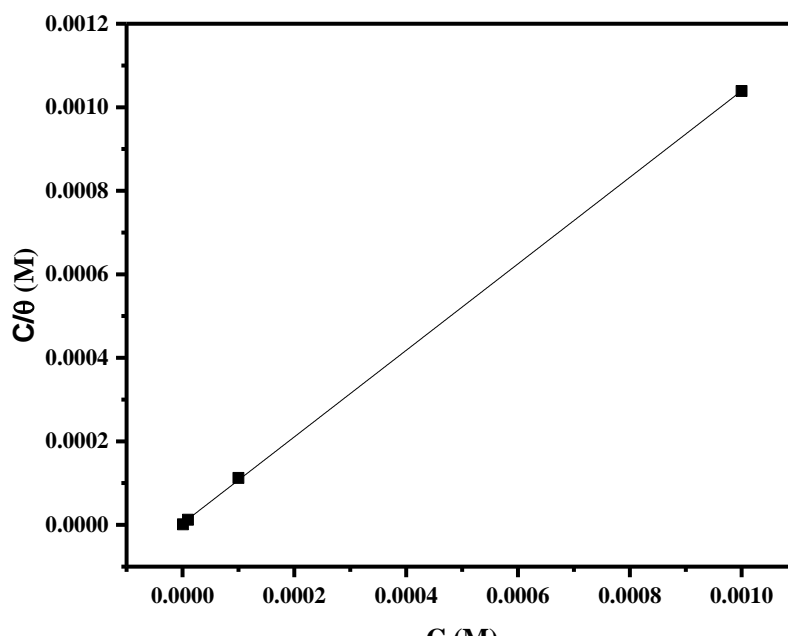
Figure 4: Langmuir adsorption of BZD-1 on the carbon steel surface in 1M HCl solution at 303K.

The value of K_{ads} obtained from the reciprocal of intercept of Langmuir isotherm line is listed in Table 3, together with the values of the Gibbs free energy of adsorption ΔG°_{ads} calculated from the equation [50]:

$$K_{ads} = \frac{1}{55.55} \exp\left(\frac{-\Delta G^{\circ}_{ads}}{RT}\right) \tag{7}$$

where R is gas constant, T is absolute temperature of experiment and the constant value of 55.55 is the concentration of water in solution in mol/l.

Large value of K_{ads} obtained for the studied inhibitor implies more efficient adsorption and hence better corrosion inhibition efficiency [11]. In general, values of ΔG_{ads}° by -20 kJ mol^{-1} are compatible with the electrostatic interaction between the charged molecules and the charged metal (physisorption) and those which are more negative than -40 kJ mol^{-1} involve charge sharing or charge transfer from the inhibitor molecules to the metal surface (chemisorptions) [2,50]. The calculated ΔG_{ads}° values for BZD-1 was found to be -41.7 kJ mol^{-1} at studied temperature (303 K), indicates that the adsorption process of inhibitor at the carbon steel surface involve the predominance of chemical adsorption.

Table 3: The values of K_{ads} and ΔG_{ads}° for carbon steel in presence of BZD-1 in 1 M HCl at 303 K.

Inhibitor	Slope	R^2	K_{ads} (L mol^{-1})	ΔG_{ads}° (kJ mol^{-1})
BZD-1	1.04	0.999	287049	-41.7

3.4. Effect of the temperature

In order to study the effect of temperature on corrosion inhibition of carbon steel in the acid reaction and to determine the activation energy of the corrosion process, the polarization curves were done at various temperatures (303-333 K) in the absence and in the presence of BZD-1 at optimal concentration (Fig. 5).
The corresponding results are given in Table 4. From these results, we can deduce that the corrosion current density in presence of inhibitor increases slightly with the increasing temperature. In return, considerable decrease was observed in the absence of the inhibitor. On the other hand, by increasing the temperature, the inhibition efficiency of BZD-1 shifted to slightly lower values indicating that BZD-1 acts as an efficient inhibitor in the range of studied temperature.
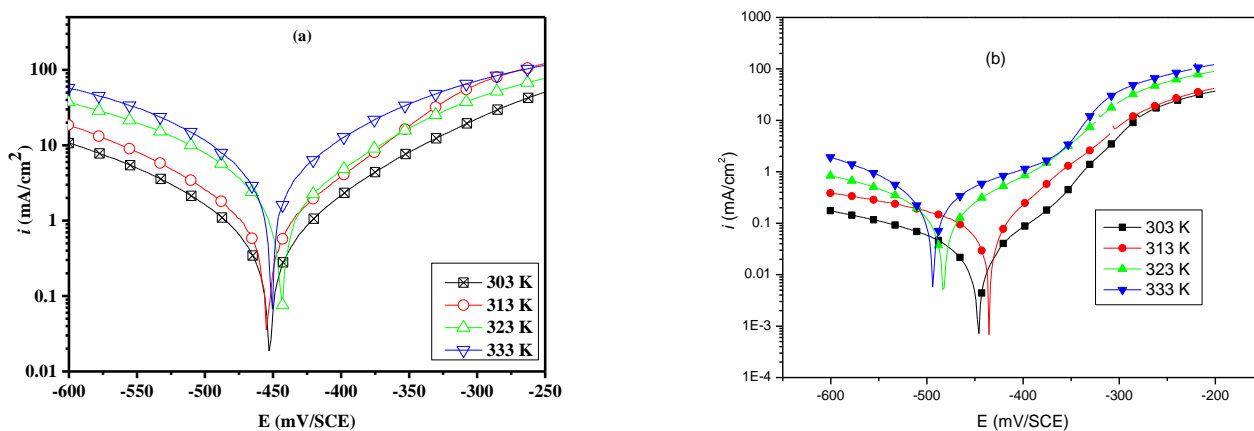
Figure 5: Potentiodynamic polarization curves for corrosion of carbon steel in 1M HCl solution in the absence and presence of 10^{-3}M of BZD-1 at different temperatures.

**Table 4:** The results of the temperature effect of C-steel corrosion performed in 1 M HCl and + 10^{-3} M BZD-1

Medium	T (K)	$-E_{corr}$ (mV/SCE)	I_{corr} (µA cm^{-2})	η_{Tafel} (%)	θ
Blank	303	452	507	—	—
	313	454	860	—	—
	323	443	1840	—	—
	333	450	2800	—	—
BZD-1	303	446	19	96	0.96
	313	435	90	90	0.90
	323	483	280	85	0.85
	333	493	570	80	0.80

The corrosion reaction can be regarded as an Arrhenius-type process; the rate is given by(8) [51]:

$$I_{corr} = k \exp\left(\frac{-E_a}{RT}\right) \quad (8)$$

where E_a is the apparent activation corrosion energy, R is the universal gas constant and k is the Arrhenius pre-exponential constant.

Arrhenius plots for the corrosion density of carbon steel in the case of tested inhibitor are given in Figure 6. Values of apparent activation energy of corrosion (E_a) for carbon steel in 1M HCl with the absence and presence of inhibitor were determined from the slope of Ln (i_{corr}) versus 1/T plots and shown in Table 5. From the results depicted in Table 5 it is observed that the value of E_a is higher (95.45 kJ/mol) in presence of BZD-1 as compared to value of E_a in the absence of BZD-1 (49.38 kJ/mol), suggesting that BZD-1 inhibits carbon steel corrosion by forming an energy barrier for corrosion process [6,13,52,53].
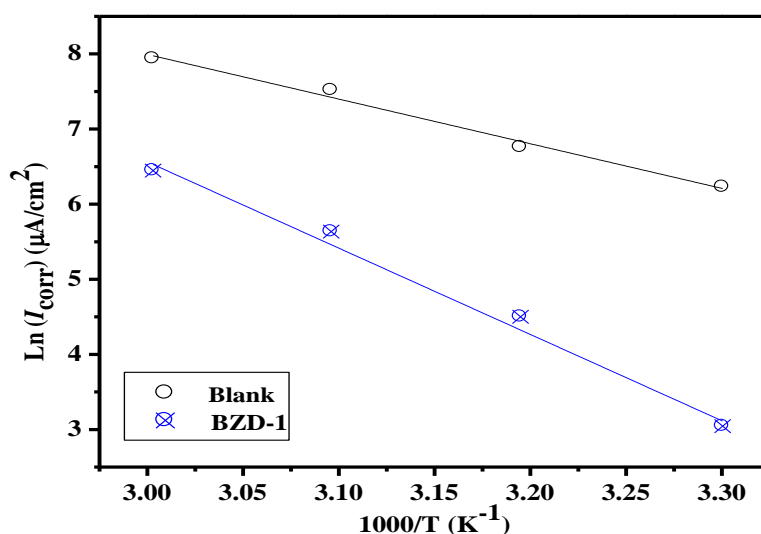
Figure 6: Arrhenius plots of Ln I_{corr} vs. 1/T for carbon steel in 1M HCl in the absence and the presence of BZD-1 at optimum concentration.
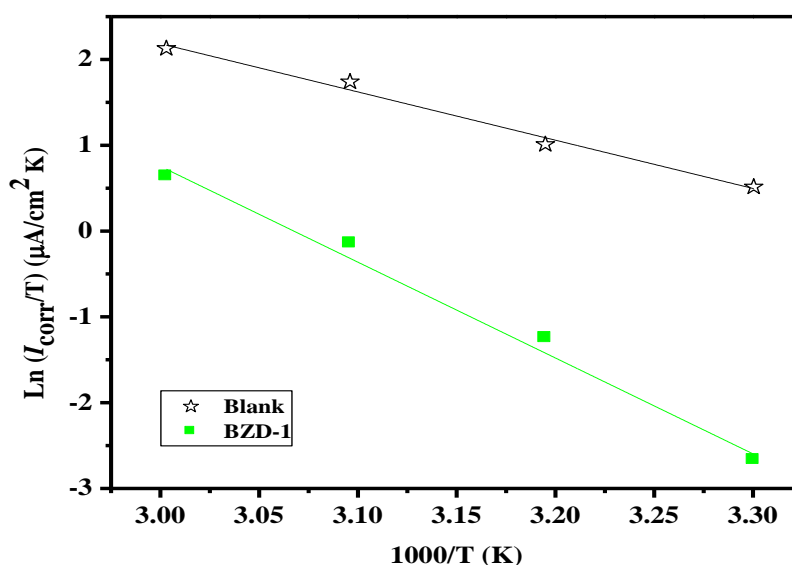
Figure 7: Transition Arrhenius plots of Ln I_{corr} vs. 1/T for carbon steel in 1M HCl in the absence and the presence of BZD-1 at optimum concentration.

Activation parameters like enthalpy (ΔH_a) and entropy (ΔS_a) for the dissolution of carbon steel in 1M HCl in the absence and presence of 10^{-3} M of BZD-1were calculated from the transition state equation [51]:

$$I_{corr} = \frac{RT}{Nh} \exp\left(\frac{\Delta S_a}{R}\right) \exp\left(\frac{-\Delta H_a}{RT}\right) \tag{9}$$

where h is Planck's constant, N is the Avogadro number, R is the universal gas constant, ΔH_a is the enthalpy of activation and ΔS_a is the entropy of activation.

Figure 7 shows that the Arrhenius plots of Ln (I_{corr}/T) versus $1/T$ gave straight lines with slope ($-\Delta H_a/R$) and intercept ($Ln\ R/Nh + \Delta S_a/R$) from where ΔH_a and ΔS_a values were calculated are given in Table 5.

Table 5: Activation parameters for the carbon steel dissolution in free 1M HCl and at 10^{-3}M of BZD-1.

Medium	E_a (kJ mol^{-1})	ΔH_a (kJ mol^{-1})	ΔS_a (J mol^{-1}K^{-1})
Blank	49.38	46.77	-38.96
BZD-1	95.45	92.82	87.36

The positive values of ΔH_a in the absence and the presence of BZD-1 reflect the endothermic nature of the carbon steel dissolution process. In addition, the value of ΔS_a were higher for inhibited solutions than that for the uninhibited solution (Table 5). This suggested that an increase in randomness occurred on going from reactants to the activated complex. This might be the results of the adsorption of organic inhibitor molecules from the hydrochloric solution could be regarded as a quasi-substitution process between the organic compound in the aqueous phase and water molecules at electrode surface [54]. In this situation, the adsorption of organic inhibitor was accompanied by desorption of water molecules from the surface. Thus the increasing in entropy of activation was attributed to the increasing in solvent entropy [55].

3.5. Quantum chemical calculations

The use of quantum chemical calculations is very important in establishing the correlation between molecular structure and corrosion inhibition efficiency. The effectiveness of an inhibitor is related to its spatial and electronic molecular structures [29]. Moreover, a theoretical study permits the pre-selection of organic compounds with the necessary structural characteristics to act as corrosion inhibitors [30]. According to frontier molecular orbital theory, only frontier molecular orbitals are involved in interaction between the reactants. Therefore, only the LUMO and HOMO of both reactants are considered for analyzing the chelation processes of chemical adsorption. The difference between the energy levels of these orbitals is important in evaluating the inhibition efficiency. Thus in the present investigation, quantum chemical calculation using $DMol^3$ was employed to explain the experimental results obtained in this study and to further give insight into the inhibition action of BZD-1 on the carbon steel surface. Fig. 8 shows the optimized geometry, the HOMO density distribution and the LUMO density distribution.

From Fig. 8, it could be seen that BZD-1 has similar HOMO and LUMO distributions, which were all located on the entire molecular structure. This is due to the presence of oxygen and nitrogen atoms together with several π-electrons on the entire molecule. Thus, the unoccupied d orbitals of Fe atom can accept electrons from inhibitor molecule to form coordinate bond. Also the inhibitor molecule can accept electrons from Fe atom with its anti-bonding orbitals to form back-donating bond. The quantum chemical calculations parameters such as; E_{HOMO}, E_{LUMO}, ΔE and ΔN are represented in Table 7. The electron affinity (EA) and ionization potential (IP) are deduced from E_{HOMO} and E_{LUMO} by the Equations (10) and (11) [30]:

$$IP = -E_{HOMO} \tag{10}$$
$$EA = -E_{LUMO} \tag{11}$$

Mulliken electronegativity (χ) and Absolute hardness (η) can be approximated using [56,57]:

$$\chi = \frac{IP + EA}{2} \tag{12}$$

$$\eta = \frac{IP - EA}{2} \tag{13}$$

The number of transferred electrons (ΔN) is calculated by application of the Pearson method using the equation [58]:

$$\Delta N = \frac{\phi - \chi_{inh}}{2(\eta_{Fe} + \eta_{inh})} \qquad (14)$$

Where ϕ is the work function of the iron surface with the value of 4.82 eV for Fe (1 1 0) [56,59], χ_{inh} is the absolute electronegativity associated to the inhibitor molecule, $\eta_{Fe} = 0$ and η_{inh} are the absolute hardness of metal and the inhibitor molecule, respectively [60,61]. The E_{HOMO} and E_{LUMO} provide information about the reactivity of the compounds. Higher the E_{HOMO} better is the ability of a molecule to donate electrons, while lower the E_{LUMO} better is the ability to accept electrons from an electron rich species [29]. The energy gap ΔE ($E_{LUMO} - E_{HOMO}$) should be small for an inhibitor for good interaction with metal surface [30]. It has also reported that the ΔN value measures the ability of a chemical compound to transfer its electrons to metal if $\Delta N > 0$ and vice versa if $\Delta N < 0$ [62,63]. In this study, the positive value of $\Delta N = 0.602$ presented in Table 6, suggest the high capability of BZD-1 to donates electrons to the MS surface.

Table 6. Quantum theoretical parameters for BZD-1 calculated using *DMol*^{3}.

| E_{HOMO} (eV)	E_{LUMO} (eV)	ΔE (eV)	ΔN_{110}
-4.522	-1.598	2.924	0.602
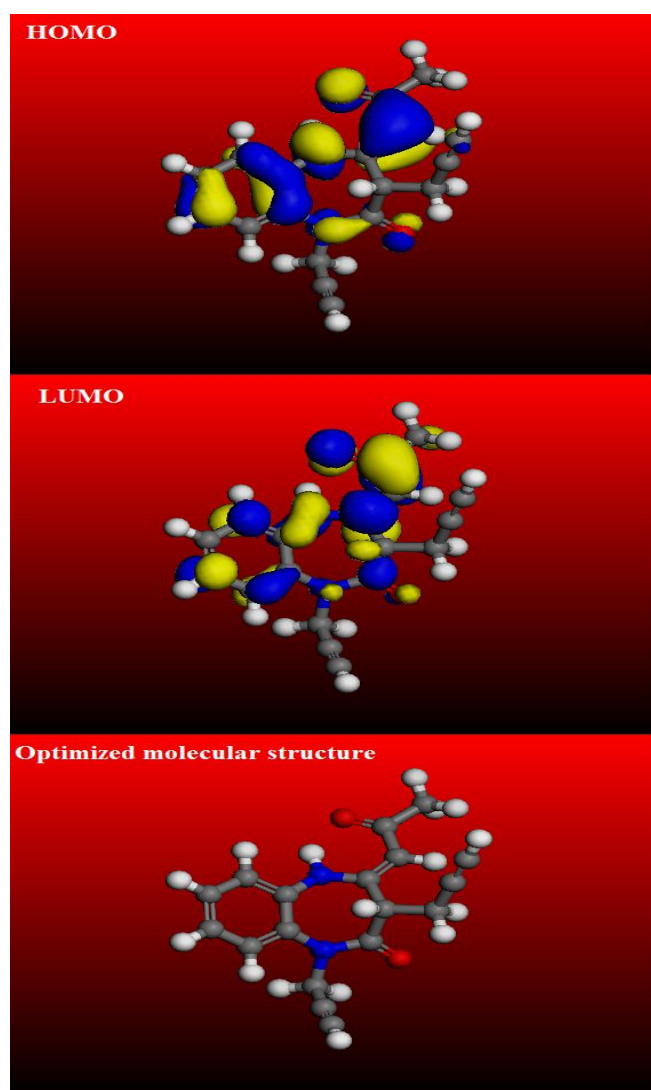
Figure 8: Frontier molecular orbital density distributions and optimized molecular structure of the synthesized inhibitor.

3.6. Monte Carlo simulations

Recently, Monte Carlo simulations has been broadly used to describe the interaction between metal and inhibitor because it provides some essential parameters such as total energy, adsorption energy, and rigid adsorption energy [64,65]. In our present study, the Monte Carlo simulations calculation was used to find the lowest energy for the investigated system. The outputs and descriptors calculated by the Monte Carlo simulations, such as the total adsorption, adsorption energy, rigid adsorption and deformation energies are presented in Table 7. Figure 9 represents the most stable low energy configuration for the adsorption of benzodiazepine derivative on Fe (110) surface obtained through the Monte Carlo simulations.

Table 7: Outputs and descriptors calculated by the Monte Carlo simulation for the lowest adsorption. Configurations of BZD-1 Fe (110) surface (in kcal/mol).

System	Total energy	Adsorption energy	Rigid adsorption energy	Deformation energy	dE_{ad}/dNi inhibitor
Fe (110)/ **BZD-1**	-124.50	-704.36	-711.04	6.68	-704.36
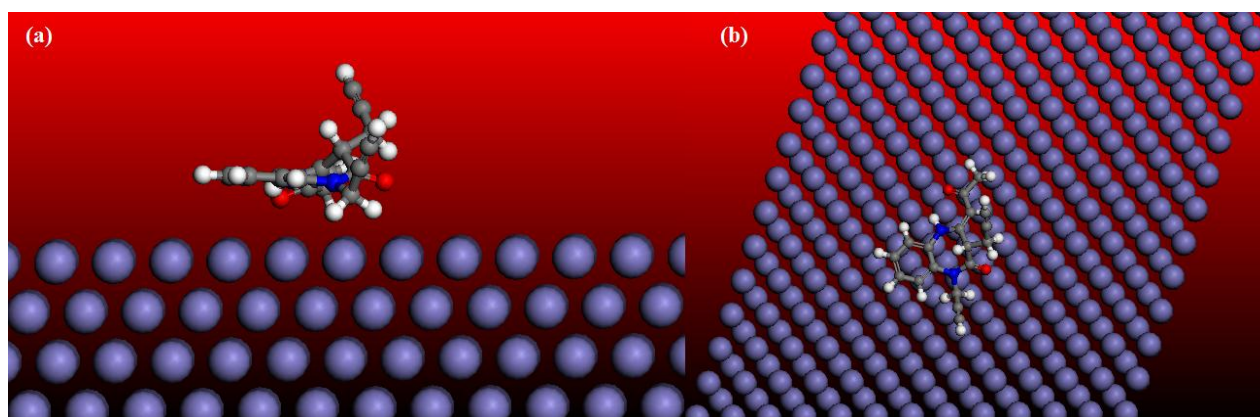
Figure 9: The side (a) and top (b) views of the most stable low energy configuration for the adsorption of the inhibitor on Fe (110) surface obtained through the Monte Carlo simulation for BZD-1.

The total energy is defined as the sum of the energies of the adsorbate components, the rigid adsorption energy and the deformation energy. In this study, the substrate energy (iron surface) is taken as zero. In addition, adsorption energy in kJ mol^{-1} reports energy released (or required) when the relaxed adsorbate components (furan derivatives) are adsorbed on the substrate. The adsorption energy is defined as the sum of the rigid adsorption energy and the deformation energy for the adsorbate components. The rigid adsorption energy reports the energy, in kJ mol^{-1}, released (or required) when the unrelaxed adsorbate components (i.e., before the geometry optimization step) are adsorbed on the substrate. The deformation energy reports the energy, in kJ mol^{-1}, released when the adsorbed adsorbate components are relaxed on the substrate surface [66]. Table 7 shows also (dE_{ads}/dNi), which reports the energy, in kJ mol^{-1}, of substrate–adsorbate configurations where one of the adsorbate components has been removed. The results depicted in Table 7 show that the benzodiazepine derivative associated with high negative values of adsorption energy resulting in the strong interactions between metal and BZD-1 molecules [66].

Conclusion

The data of present investigation reveal that benzodiazepine derivative is a good inhibitor for carbon steel in 1M HCl solution. The inhibition efficiency increases with the concentration of BZD-1 while it decreases slightly with rise in temperature. Polarization measurements show that BZD-1 inhibit both the anodic and cathodic processes indicating that this is mixed type corrosion inhibitor. EIS measurements depict that the charge transfers resistance increases and double layer capacitance declines in the presence of BZD-1, confirming the adsorption of inhibitor molecules on the carbon steel surface. The adsorption of the BZD-1 on the carbon steel surface in hydrochloric acid solution obeys the Langmuir adsorption isotherm. The large negative value of adsorption energy in Monte Carlo simulations indicates the strong interaction between the metal and the investigated inhibitor.

References

1. El Makrini B., Lgaz H., Toumiat K., Salghi R., Jodeh S., Hanbali G., Belkhaouda M., Zougagh M., *Res J Pharm Biol Chem Sci* **7** (2016) 2277.
2. Adardour L., Lgaz H, Salghi R, Larouj M, Jodeh S, Zougagh M, Hamed O, Oudda H. *Pharm Lett* 8 (2016) 212.
3. Ismaily Alaoui K., El Hajjaji F., Azaroual M.A., Taleb M., Chetouani A., Hammouti B., Abrigach F., Khoutoul M., Abboud Y., Aouniti A., Touzani R., *J. Chem. Pharmac. Res.*, 6 N°7 (2014) 63-81
4. Lgaz H., Anejjar A, Salghi R, Jodeh S, Zougagh M, Warad I, Larouj M, Sims P. *Int J Corros Scale Inhib* **5** (2016) 209.
5. Bousskri A., Anejjar A., Salghi R, Jodeh S, Touzani R, Bazzi L, Lgaz H. *J Mater Environ Sci* **7** (2016) 4269.
6. Saadouni M., Larouj M., Salghi R., Lgaz H, Jodeh S, Zougagh M, Souizi A. *Pharm Lett* **8** (2016) 6.
7. Adardour L., Lgaz H., Salghi R., Larouj M, Jodeh S, Zougagh M, Hamed O, Taleb M. *Pharm Lett* **8** (2016) 173.
8. Adardour L., Lgaz H., Salghi R., Larouj M, Jodeh S, Zougagh M, Warad I, Oudda H. *Pharm Lett* **8** (2016) 126.
9. El Makrini B., Toumiat K, Lgaz H, Salghi R, Jodeh S, Hanbali G, Belkhaouda M, Zougagh M. *Res J Pharm Biol Chem Sci* **7** (2016) 2286.
10. Adardour L., Larouj M, Lgaz H, Belkhaouda M, Salghi R, Jodeh S, Salman A, Oudda H, Taleb M. *Pharma Chem* 8 (2016) 152.
11. Lgaz H., Salghi R, Jodeh S, Hammouti B. *J Mol Liq* 225 (2017) 271.
12. Toumiat K., El Aoufir Y, Lgaz H, Salghi R, Jodeh S, Zougagh M, Oudda H. *Res J Pharm Biol Chem Sci* 7(2016) 1210.
13. Saadouni M., Larouj M, Salghi R, Lgaz H, Jodeh S, Zougagh M, Souizi A. *Pharm Lett* 8 (2016) 96.
14. El Makrini B., Larouj M, Lgaz H, Salghi R, Salman A, Belkhaouda M, Jodeh S, Zougagh M, Oudda H. *Pharma Chem* 8 (2016) 227.
15. El Aoufir Y, Lgaz H, Toumiat K, Salghi R, Jodeh S, Zougagh M, Guenbour A, Oudda H. *Res J Pharm Biol Chem Sci* 7 (2016) 1200.
16. Lgaz H., Saadouni M, Salghi R, Jodeh S, Elfaydy M, Lakhrissi B, Boukhris S, Oudda H. *Pharm Lett* 8 (2016) 158.
17. Toumiat K., El Aoufir Y, Lgaz H, Salghi R, Jodeh S., Zougagh M, Oudda H. *Res J Pharm Biol Chem Sci* 7 (2016) 1209.
18. El Aoufir Y., Lgaz H, Toumiat K, Salghi R, Jodeh S, Zougagh M, Guenbour A, Oudda H. *Res J Pharm Biol Chem Sci* 7(2016) 1219.
19. Ghazoui A., Zarrouk A., Bencaht N., Salghi R., Assouag M., El Hezzat M., Guenbour A., Hammouti B., *J. Chem. Pharm. Res*. 6 (2014) 704.
20. Zarrok H., Zarrouk A., Salghi R., Ramli Y., Hammouti B., Al-Deyab S.S., Essassi E.M., Oudda H., *Int. J. Electrochem. Sci*. 7(9) (2012) 8958.
21. Bendaha H., Zarrouk A., Aouniti A., Hammouti B., El Kadiri S., Salghi R., Touzan R., *Phys. Chem. News* 64 (2012) 95.
22. Zarrouk A., Hammouti B., Zarrok H., Salghi R., Dafali A., Bazzi L., Bammou L., Al-Deyab S.S., *Der Pharm. Chem*. 4(1) (2012) 337.
23. Ghazoui A., Saddik R., Benchat N., Hammouti B., Guenbour M., Zarrouk A., Ramdani M., *Der Pharm. Chem*. 4(1) (2012) 352.
24. Zarrouk A., Hammouti B., Zarrok H., Bouachrine M., Khaled K.F., Al-Deyab S.S., *Int. J. Electrochem. Sci*. 6 (2012) 89.
25. Zarrok H., Zarrouk A., Salghi R., Assouag M., Hammouti B., Oudda H., Boukhris S., Al Deyab S.S., Warad I., *Der Pharm. Lett*. 5 (2013) 43.
26. Zarrok H., Saddik R., Oudda H., Hammouti B., El Midaoui A., Zarrouk A., Benchat N., Ebn Touhami M., *Der Pharm. Chem*. 3(5) 2011) 272.
27. Zarrouk A., Hammouti B., Touzani R., Al-Deyab S.S., Zertoubi M., Dafali A., Elkadiri S., *Int. J. Electrochem. Sci*. 6 (10) (2011) 4939.
28. Larouj M., Belkhaouda M., Lgaz H, Salghi R, Jodeh S, Samhan S, Serrar H, Boukhris S, Zougagh M, Oudda H. *Pharma Chem* 8(2016) 114.
29. Ghazoui A., Benchat N., El-Hajjaji F., Taleb M., Rais Z., Saddik R., Elaatiaoui A., Hammouti B., *Journal of Alloys and Compounds*, 693 (2017) 510-517

30. Jafari H., Danaee I., Eskandari H., RashvandAvei M. *J Mater Sci Technol* 30(2014) 239.
31. ElHajjaji F., Greche H., Taleb M., Chetouani A., Aouniti A., Hammouti B., *J. Mater. Environ. Sci.* 7 (2) (2016) 566-578.
32. Niouri W., Zerga B., Sfaira M, Taleb M, Touhami ME, Hammouti B, Mcharfi M, Al-Deyab S, Benzeid H, Essassi E.M. *Int J Electrochem Sci* 9(2014) 8283.
33. Niouri W, Zerga B, Sfaira M, Taleb M, Hammouti B, Touhami ME, Al-Deyab S, Benzeid H, Essassi EM. *Int J Electrochem Sci* 7(2012) 10190.
34. Özcan M., Karadağ F, Dehri I. *Colloids Surf Physicochem Eng Asp* 316(2008) 55.
35. Şahin M., Gece G, Karcı F, Bilgic S. *J Appl Electrochem* 38(2008) 809.
36. Sebhaoui J., El Bakri Y., Rayni I, Essassi EM, Mague JT. *IUCrData* 1(2016) 161013.
37. Delley B. J Chem Phys 113(2000) 7756.
38. Materials Studio. Revision 6.0. Accelrys Inc., San Diego, USA (2013).
39. Mulliken R.S. I. J Chem Phys 23(1955) 1833.
40. Kaya S., Tüzün B, Kaya C, Obot IB. *J Taiwan Inst Chem Eng* 58(2016) 528.
41. Khaled K.F., El-Maghraby A. *Arab J Chem* 7(2014) 319–326.
42. Wang X., Wang Q, Wan Y, Ma Y. *Int J Electrochem Sci* 11(2016) 6229.
43. Lgaz H., Salghi R, Larouj M, Elfaydy M, Jodeh S, Rouifi Z, Lakhrissi B, Oudda H., *J. Mater Environ. Sci .* 7 (2016) 4471.
44. Elfaydy M, Lgaz H, Salghi R, Larouj M, Jodeh S, Rbaa M, Oudda H, Toumiat K, Lakhrissi B. *J Mater Environ Sci* 7(2016) 3193.
45. Popova A., Christov M, Vasilev A., *Corros. Sci*. 53 (2011) 1770.
46. Ramezanzadeh B., Arman S.Y., Mehdipour M., Markhali B.P., *Appl. Surf. Sci*. 289 (2014) 129.
47. Lopez D.A., Simison S.N., de Sanchez S.R., *Electrochimica Acta* 48 (2003) 845.
48. Martinez S., Metikoš-Huković M., *J. Appl. Electrochem.* 33 (2003) 1137.
49. Verma C., Quraishi MA, Ebenso EE, Obot IB, El Assyry A. *J Mol Liq* 219(2016) 647.
50. Hmamou DB, Salghi R, Zarrouk A, Zarrok H, Touzani R, Hammouti B, El Assyry A. *J Environ Chem Eng* 3(2015) 2031.
51. Bahrami M.J., Hosseini SMA, Pilvar P. *Corros Sci* 52 (2010) 2793.
52. Verma C., Quraishi MA, Singh A. *J Mol Liq* 212 (2015) 804.
53. Verma C., Ebenso EE, Bahadur I, Obot IB, Quraishi MA. *J Mol Liq* 212 (2015) 209.
54. Zarrouk A., Hammouti B., Dafali A., F. Bentiss, *Ind. Eng. Chem. Res*. 52 (2013) 2560.
55. Ateya B., El-Anadouli B.E., El-Nizamy F.M., *Corros. Sci*. 24 (1984) 509.
56. Pearson R.G. *Inorg Chem* 27 (1988) 734–740.
57. Sastri V., Perumareddi J. *Corrosion* 53 (1997) 617.
58. Martinez S. *Mater Chem Phys* 77 (2003) 97.
59. Lukovits I., Kalman E, Zucchi F. *Corrosion* 57 (2001) 3.
60. Cao Z., Tang Y, Cang H, Xu J, Lu G, Jing W. *Corros Sci* 83 (2014) 292.
61. Kokalj A., *Chem Phys* 393 (2012) 1.
62. Kokalj A. *Electrochimica Acta* 56 (2010) 745.
63. Kovačević N., Kokalj A. *Corros Sci* 53 (2011) 909.
64. Eivani A.R., Zhou J., Duszczyk J. *Comput Mater Sci* 54 (2012) 370.
65. John S., Joseph A., Sajini T., James Jose A., *Egypt. J. Pet.* (2016) doi:10.1016/j.ejpe.2016.10.005
66. Khaled K.F., El-Maghraby A., *Arab J Chem* 7 (2014) 319.

(2017) ; http://www.jmaterenvironsci.com